

AN ADAPTIVE NON-SYMMETRIC FINITE VOLUME AND BOUNDARY ELEMENT COUPLING METHOD FOR A FLUID MECHANICS INTERFACE PROBLEM

CHRISTOPH ERATH AND ROBERT SCHORR

ABSTRACT. We consider an interface problem often arising in transport problems: a coupled system of partial differential equations with one (elliptic) transport equation on a bounded domain and one equation (in this case the Laplace problem) on the complement, an unbounded domain. Based on the non-symmetric coupling of the finite volume method and boundary element method of [EOS15] we introduce a robust residual error estimator. The upper bound of the error in an energy (semi)norm is robust against variation of the model data. The lower bound, however, additionally depends on the Péclet number. In several examples we use the local contributions of the a posteriori error estimator to steer an adaptive mesh-refining algorithm. The adaptive FVM-BEM coupling turns out to be an efficient method especially to solve problems from fluid mechanics, mainly because of the local flux conservation and the stable approximation of convection dominated problems.

Keywords. finite volume method, boundary element method, non-symmetric coupling, convection dominated, robust a posteriori error estimates, adaptive mesh refinement

Mathematics subject classification. 65N08, 65N38, 65N15, 65N50, 76M12, 76M15

1. INTRODUCTION AND MODEL PROBLEM

We consider the prototype for flow and transport in porous media in an interior domain and a homogeneous diffusion process in the corresponding unbounded exterior problem. To approximate such problems the coupling of the finite volume method (FVM) and the boundary element method (BEM) is of particular interest. For the vertex-centered FVM-BEM we refer to [Era12] and for the cell-centered FVM-BEM to [Era13a]. Note that the coupling of FVM and BEM conserves mass, provides a stable approximation also for convection dominated problems (option of an upwind stabilization) in the interior domain, and avoids the truncation of the unbounded exterior domain due to a transformation of the exterior problem into an integral equation. We can also interpret the model that the (unbounded) exterior problem “replaces” the (unknown) boundary conditions of the interior problem [Era12, Remark 2.1]. Recently, the non-symmetric vertex-centered FVM-BEM coupling approach was introduced in [EOS15], which results in a smaller system of linear equations than the previous three field coupling approach cited above. However, a posteriori estimators for this kind of FVM-BEM coupling were not developed. Note that for uniform mesh refinement, optimal convergence order can only be guaranteed if the solution has enough regularity [EOS15], which is usually

Date: November 26, 2021.

C. Erath (corresponding author): TU Darmstadt, Germany; erath@mathematik.tu-darmstadt.de.

R. Schorr: TU Darmstadt, Germany; schorr@gsc.tu-darmstadt.de.

not met in practice. Computable local contributions of a posteriori estimators can be used to refine a mesh for a numerical scheme, where the error appears to be large and thus might lead to an improved convergence rate.

In general, a posteriori estimators bound the error from above (reliability) and below (efficiency). Probably the most widespread a posteriori estimates are of residual type; see, e.g., [Ver96] for a survey in the context of finite element methods (FEM) for the Poisson problem. Estimators for FEM-BEM couplings are also well-established. In [AFF⁺13] the authors provide a good overview of residual-based a posteriori estimates for different FEM-BEM coupling strategies, also for a non-symmetric FEM-BEM coupling, but only for a diffusion operator. Since we consider a convection diffusion reaction problem, we have a special focus on robust estimates, i.e., estimates which should not depend on the variation of the diffusion, dominated convection and reaction. Additionally, we do not assume a strong coerciveness assumption for the convection reaction terms. Note that the estimates have to be done in a certain energy (semi)norm. Therefore, the ellipticity estimate for a stabilized bilinear form of the problem from [EOS15, Theorem 4] (or [OS13, AFF⁺13] for pure diffusion problems) is not directly applicable since the dependency of the constant can not be stated explicitly for an estimate in the energy (semi)norm. Thus, we prove an ellipticity estimate in the energy (semi)norm for the original bilinear form in Lemma 2. This estimate is only valid if the minimal eigenvalue is bigger than a computable bound, which depends on an arbitrary but fixed $\varepsilon \in (0, 1)$ and the contraction constant of the double layer integral operator. Similar to the discussion in [OS13, AFF⁺13, EOS15] this seems to be a theoretical restriction. Finally, our constant of the ellipticity estimate depends on the minimal eigenvalue of the diffusion matrix and ε . However, if we know the minimal eigenvalue we can calculate the constant explicitly. Hence, in the following we consider this estimate as robust having chosen the diffusion big enough; see Remark 8. The proof of reliability relies on a robust interpolation operator known from the finite element literature [Pet02]. Note that the diffusion distribution has to be quasi-monotone over a primal triangulation. Thus, to simplify notation, we present the robust estimator only for piecewise constant diffusion. Contrary to the analysis in [Era13b] the proof starts with the robust ellipticity estimate. Since our system does not provide a “global” Galerkin orthogonality (in contrast to a classical FEM-BEM coupling) we use an L^2 -orthogonality property of the residual to integrate a piecewise constant approximation of the error and add and subtract the robust interpolation of the error. This allows us to use some robust estimates of residual and jump terms; see [Era13b]. Furthermore, the Galerkin orthogonality of the BEM part and some standard localizations complete the proof and show Theorem 7. Note that the fully computable, robust local refinement indicators consist of a residual and normal jump quantities (including jump terms on the coupling boundary) with factors, which ensure robustness. A tangential jump measures the error in tangential direction on the coupling boundary. The upwind stabilization adds an additional quantity to our estimator, which measures the amount of upwinding. To complete the theory we also state a non-robust version of an estimator in Theorem 9. There, we directly use the ellipticity estimate of [EOS15, Theorem 4] for a stabilized bilinear form. As in [AFF⁺13] for a pure diffusion operator we show that this stabilized bilinear form evaluated for the errors is equal to the standard bilinear form. The rest of the proof is standard and follows the lines above using non-robust techniques such as the classical Clément nodal interpolant [Clé75]. We remark that in this case the quasi-monotonicity of the diffusion is not necessary.

The efficiency follows mostly from [Era13b] and is stated in Theorem 12. Therefore, we only present the local estimate from a contribution which differs. In summary, the estimator is local and, in case of a quasi-uniform mesh on the boundary, also generically efficient. We stress that even for the FEM-BEM coupling there is no better result available in the literature [AFF⁺13]. However, the lower bound is indeed robust against discontinuities of the diffusion coefficient and a dominating reaction term but still depends on the local Péclet number for convection problems. This property is typical for estimates in the energy norm. To get fully robustness one would have to introduce additionally an augmented norm, which absorbs the convection terms. We note, however, that this norm is not computable and we could not prove an upper bound for this extended norm because we do not have homogeneous Dirichlet boundary conditions. For more details we refer to [Era13b, Remark 6.1.].

Throughout, we denote by $L^m(\cdot)$ and $H^m(\cdot)$, $m > 0$, the standard Lebesgue and Sobolev spaces equipped with the corresponding norms $\|\cdot\|_{L^2(\cdot)}$ and $\|\cdot\|_{H^m(\cdot)}$. Our domain $\Omega \subset \mathbb{R}^d$, $d = 2, 3$ will be a bounded domain with connected polygonal Lipschitz boundary Γ . For $\omega \subset \Omega$, $(\cdot, \cdot)_\omega$ is the L^2 scalar product. The space $H^{m-1/2}(\Gamma)$ is the space of all traces of functions from $H^m(\Omega)$ and the duality between $H^m(\Gamma)$ and $H^{-m}(\Gamma)$ is given by the extended L^2 -scalar product $\langle \cdot, \cdot \rangle_\Gamma$. In $H_{\text{loc}}^1(\Omega) := \{v : \Omega \rightarrow \mathbb{R} \mid v|_K \in H^1(K), \text{ for all } K \subset \Omega \text{ open and bounded}\}$ we collect all functions with local H^1 behavior. Furthermore, the Sobolev space $W^{1,\infty}$ contains exactly the Lipschitz continuous functions. If it is clear from the context, we do not use a notational difference for functions in a domain and their traces. To simplify the presentation we equip the space $\mathcal{H} := H^1(\Omega) \times H^{-1/2}(\Gamma)$ with the norm

$$\|\mathbf{v}\|_{\mathcal{H}}^2 := \|v\|_{H^1(\Omega)}^2 + \|\psi\|_{H^{-1/2}(\Gamma)}^2$$

for $\mathbf{v} = (v, \psi) \in \mathcal{H}$.

This allows us to specify our model problem in detail. Let Ω be defined as above and let $\Omega_e = \mathbb{R}^d \setminus \overline{\Omega}$ be the corresponding unbounded exterior domain. The coupling boundary $\Gamma = \partial\Omega = \partial\Omega_e$ is divided in an inflow and outflow part, namely $\Gamma^{\text{in}} := \{x \in \Gamma \mid \mathbf{b}(x) \cdot \mathbf{n}(x) < 0\}$ and $\Gamma^{\text{out}} := \{x \in \Gamma \mid \mathbf{b}(x) \cdot \mathbf{n}(x) \geq 0\}$, respectively, where \mathbf{n} is the normal vector on Γ pointing outward with respect to Ω .

We consider the same model problem as in [Era12, Era13a, EOS15] which reads in a weak sense: find $u \in H^1(\Omega)$ and $u_e \in H_{\text{loc}}^1(\Omega_e)$ such that

$$\operatorname{div}(-\mathbf{A}\nabla u + \mathbf{b}u) + cu = f \quad \text{in } \Omega, \quad (1a)$$

$$-\Delta u_e = 0 \quad \text{in } \Omega_e, \quad (1b)$$

$$u_e(x) = C_\infty \log|x| + \mathcal{O}(1/|x|) \quad \text{for } |x| \rightarrow \infty, \quad d = 2, \quad (1c)$$

$$u_e(x) = \mathcal{O}(1/|x|) \quad \text{for } |x| \rightarrow \infty, \quad d = 3, \quad (1d)$$

$$u = u_e + u_0 \quad \text{on } \Gamma, \quad (1e)$$

$$(\mathbf{A}\nabla u - \mathbf{b}u) \cdot \mathbf{n} = \frac{\partial u_e}{\partial \mathbf{n}} + t_0 \quad \text{on } \Gamma^{\text{in}}, \quad (1f)$$

$$(\mathbf{A}\nabla u) \cdot \mathbf{n} = \frac{\partial u_e}{\partial \mathbf{n}} + t_0 \quad \text{on } \Gamma^{\text{out}}. \quad (1g)$$

The diffusion matrix $\mathbf{A} : \Omega \rightarrow \mathbb{R}^{d \times d}$ has piecewise Lipschitz continuous entries; i.e., entries in $W^{1,\infty}(T)$ for every $T \in \mathcal{T}$, where \mathcal{T} is a mesh of Ω introduced below in subsection 3.1.

Additionally, \mathbf{A} is bounded, symmetric and uniformly positive definite, i.e., there exist positive constants $C_{\mathbf{A},1}$ and $C_{\mathbf{A},2}$ with $C_{\mathbf{A},1}|\mathbf{v}|^2 \leq \mathbf{v}^T \mathbf{A}(x) \mathbf{v} \leq C_{\mathbf{A},2}|\mathbf{v}|^2$ for all $\mathbf{v} \in \mathbb{R}^d$ and almost every $x \in \Omega$. The best constant $C_{\mathbf{A},1}$ equals the infimum over $x \in \Omega$ of the minimum eigenvalue of $\mathbf{A}(x)$, which we will denote $\lambda_{\min}(\mathbf{A})$. Note that this includes coefficients \mathbf{A} that are \mathcal{T} -piecewise constant. Furthermore, $\mathbf{b} \in W^{1,\infty}(\Omega)^d$ and $c \in L^\infty(\Omega)$ satisfy the weak coerciveness assumption

$$\frac{1}{2} \operatorname{div} \mathbf{b}(x) + c(x) \geq 0 \quad \text{for almost every } x \in \Omega. \quad (2)$$

We stress that our analysis holds for constant \mathbf{b} and $c = 0$ as well. Finally, we choose the right-hand side $f \in L^2(\Omega)$, and allow prescribed jumps $u_0 \in H^{1/2}(\Gamma)$, and $t_0 \in H^{-1/2}(\Gamma)$. In the two dimensional case we additionally assume $\operatorname{diam}(\Omega) < 1$ which can always be achieved by scaling to ensure $H^{-1/2}(\Gamma)$ ellipticity of the single layer operator defined below. The constant C_∞ is unknown; see [McL00, Era12, EOS15] for possible different radiation conditions. The model problem (1) admits a unique solution for both, the two and three dimensional case; see [Era12].

The content of this paper is organized as follows. Section 2 gives a short summary on integral equations and the weak formulation of our model problem based on the non-symmetric coupling approach. In section 3 we introduce the non-symmetric FVM-BEM coupling to solve our model problem. Section 4 introduces a robust a posteriori error estimator and shows reliability and efficiency. Numerical experiments, found in section 5, confirm the theoretical findings. Some conclusions complete the work.

2. INTEGRAL EQUATION AND WEAK COUPLING FORMULATION

We consider a weak form of the model problem (1) in terms of boundary integral operators [EOS15]. Then the coupling reads: find $u \in H^1(\Omega)$, $\phi \in H^{-1/2}(\Gamma)$ such that

$$\mathcal{A}(u, v) - \langle \phi, v \rangle_\Gamma = (f, v)_\Omega + \langle t_0, v \rangle_\Gamma, \quad (3a)$$

$$\langle \psi, (1/2 - \mathcal{K})u \rangle_\Gamma + \langle \psi, \mathcal{V}\phi \rangle_\Gamma = \langle \psi, (1/2 - \mathcal{K})u_0 \rangle_\Gamma \quad (3b)$$

for all $v \in H^1(\Omega)$, $\psi \in H^{-1/2}(\Gamma)$ with the bilinear form

$$\mathcal{A}(u, v) := (\mathbf{A} \nabla u - \mathbf{b}u, \nabla v)_\Omega + (cu, v)_\Omega + \langle \mathbf{b} \cdot \mathbf{n} u, v \rangle_{\Gamma^{out}}.$$

The single layer operator \mathcal{V} and the double layer operator \mathcal{K} are given, for smooth enough input, by

$$(\mathcal{V}\psi)(x) = \int_\Gamma \psi(y) G(x-y) ds_y \quad (\mathcal{K}\theta)(x) = \int_\Gamma \theta(y) \frac{\partial}{\partial \mathbf{n}_y} G(x-y) ds_y \quad x \in \Gamma,$$

where \mathbf{n}_y is a normal vector with respect to y and $G(z) = -\frac{1}{2\pi} \log |z|$ for the 2-D case and $G(z) = \frac{1}{4\pi} \frac{1}{|z|}$ for the 3-D case is the fundamental solution for the Laplace operator. We recall [Cos88, Theorem 1] that these operators can be extended to bounded operators

$$\mathcal{V} \in L(H^{s-1/2}(\Gamma); H^{s+1/2}(\Gamma)), \quad \mathcal{K} \in L(H^{s+1/2}(\Gamma); H^{s+1/2}(\Gamma)), \quad s \in [-\frac{1}{2}, \frac{1}{2}].$$

It is also well-known that \mathcal{V} is symmetric and $H^{-1/2}(\Gamma)$ elliptic. The expression

$$\|\cdot\|_{\mathcal{V}}^2 := \langle \mathcal{V}\cdot, \cdot \rangle_\Gamma$$

defines a norm in $H^{-1/2}(\Gamma)$. This norm is equivalent to $\|\cdot\|_{H^{-1/2}(\Gamma)}$. In this work, we will also use the contraction constant $C_K \in [1/2, 1)$ from [SW01] for the double layer operator \mathcal{K} .

For convenience the system (3a)–(3b) can be written in the product space $\mathcal{H} = H^1(\Omega) \times H^{-1/2}(\Gamma)$ as follows: we introduce the bilinear form $\mathcal{B} : \mathcal{H} \times \mathcal{H} \rightarrow \mathbb{R}$

$$\mathcal{B}((u, \phi); (v, \psi)) := \mathcal{A}(u, v) - \langle \phi, v \rangle_\Gamma + \langle \psi, (1/2 - \mathcal{K})u \rangle_\Gamma + \langle \psi, \mathcal{V}\phi \rangle_\Gamma, \quad (4)$$

and the linear functional

$$F((v, \psi)) := (f, v)_\Omega + \langle t_0, v \rangle_\Gamma + \langle \psi, (1/2 - \mathcal{K})u_0 \rangle_\Gamma. \quad (5)$$

Then (3a)–(3b) is equivalent to: find $\mathbf{u} \in \mathcal{H}$ such that

$$\mathcal{B}(\mathbf{u}; \mathbf{v}) = F(\mathbf{v}) \quad \text{for all } \mathbf{v} \in \mathcal{H}. \quad (6)$$

3. A NON-SYMMETRIC FVM-BEM COUPLING

In this section we shortly present the non-symmetric FVM-BEM coupling discretization introduced in [EOS15]. From now on we assume $t_0 \in L^2(\Gamma)$. First, let us introduce the notation for the triangulation and some discrete function spaces.

3.1. Triangulation. Throughout, \mathcal{T} denotes a triangulation or primal mesh of Ω , \mathcal{N} and \mathcal{E} are the corresponding set of nodes and edges/faces, respectively. The elements $T \in \mathcal{T}$ are non-degenerate triangles (2-D case) or tetrahedra (3-D case), and considered to be closed. For the Euclidean diameter of $T \in \mathcal{T}$ we write $h_T := \sup_{x, y \in T} |x - y|$. Moreover, h_E denotes the length of an edge or Euclidean diameter of $E \in \mathcal{E}$. The triangulation is regular in the sense of Ciarlet [Cia78], i.e., the ratio of the diameter h_T of any element $T \in \mathcal{T}$ to the diameter of its largest inscribed ball is bounded by a constant independent of h_T , the so called shape-regularity constant. Additionally, we assume that the triangulation \mathcal{T} is aligned with the discontinuities of the coefficients \mathbf{A} , \mathbf{b} , and c of the differential equation (if any) and of the data f , u_0 , and t_0 . Throughout, if \mathbf{n} appears in a boundary integral, it denotes the unit normal vector to the boundary pointing outward the domain. We denote by $\mathcal{E}_T \subset \mathcal{E}$ the set of all edges/faces of T , i.e., $\mathcal{E}_T := \{E \in \mathcal{E} \mid E \subset \partial T\}$ and by $\mathcal{E}_\Gamma := \{E \in \mathcal{E} \mid E \subset \Gamma\}$ the set of all edges/faces on the boundary Γ .

Dual mesh. We construct the dual mesh \mathcal{T}^* from the primal mesh \mathcal{T} as follows. In two dimensions we connect the center of gravity of an element $T \in \mathcal{T}$ with the midpoint of the edges $E \in \mathcal{E}_T$; see Figure 1(a), where the dashed lines are the new boxes, called control volumes. In three dimensions we connect the center of gravity of an element $T \in \mathcal{T}$ with the centers of gravity of the four faces $E \in \mathcal{E}_T$. Furthermore, each center of gravity of a face $E \in \mathcal{E}_T$ is connected by straight lines to the midpoints of its edges. The elements of this dual mesh \mathcal{T}^* are taken to be closed. Note that they are non-degenerate domains because of the non-degeneracy of the elements of the primal mesh. Given a vertex $a_i \in \mathcal{N}$ from the primal mesh \mathcal{T} ($i = 1 \dots \#\mathcal{N}$), there exists a unique box containing a_i . We thus number the elements of the dual mesh $V_i \in \mathcal{T}^*$, following the numbering of vertices.

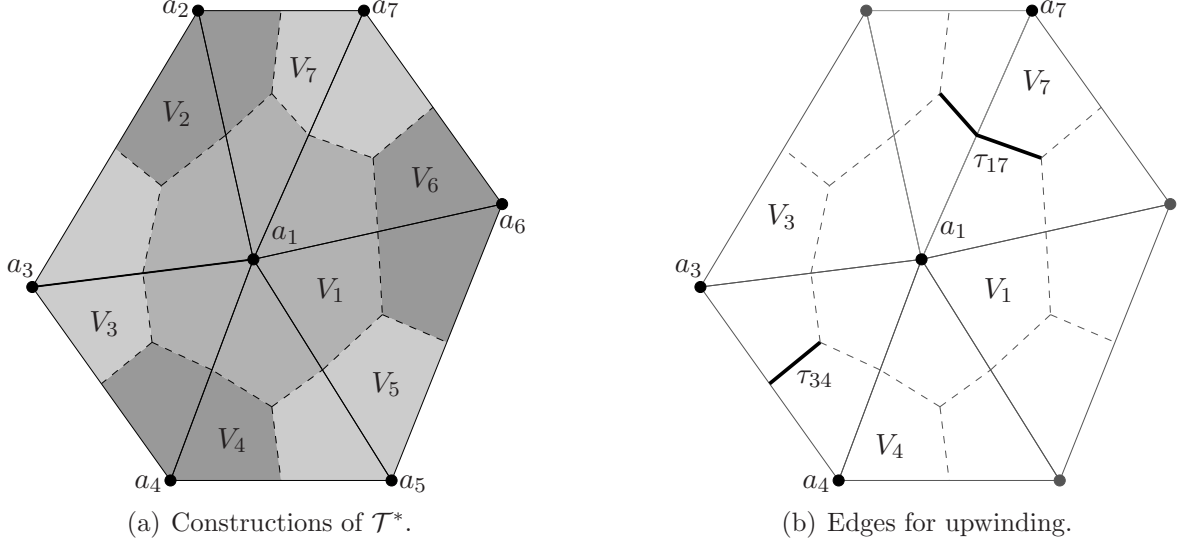


FIGURE 1. The construction of the dual mesh \mathcal{T}^* from the primal mesh \mathcal{T} in two dimensions with the center of gravity point in the interior of the elements in Figure (a); the dashed lines (gray boxes) are the new control volumes V_i of \mathcal{T}^* and are associated with $a_i \in \mathcal{N}$. In Figure (b) we see an example intersection $\tau_{17} = V_1 \cap V_7 \neq \emptyset$ of two neighboring cells $V_1, V_7 \in \mathcal{T}^*$, where τ_{17} is the union of two straight segments. For $a_3, a_4 \in \mathcal{N}$, where both a_3 and a_4 lie on Γ , $\tau_{34} = V_3 \cap V_4 \neq \emptyset$ is only a single segment.

Discrete function spaces. We define by $\mathcal{S}^1(\mathcal{T}) := \{v \in \mathcal{C}(\Omega) \mid v|_T \text{ affine for all } T \in \mathcal{T}\}$ the piecewise affine and globally continuous function space on \mathcal{T} . The space $\mathcal{P}^0(\mathcal{E}_\Gamma)$ is the \mathcal{E}_Γ -piecewise constant function space. On the dual mesh \mathcal{T}^* we provide $\mathcal{P}^0(\mathcal{T}^*) := \{v \in L^2(\Omega) \mid v|_V \text{ constant } V \in \mathcal{T}^*\}$. With the aid of the characteristic function χ_i^* over the volume V_i we can write $v_h^* \in \mathcal{P}^0(\mathcal{T}^*)$ as

$$v_h^* = \sum_{x_i \in \mathcal{N}} v_i^* \chi_i^*,$$

with real coefficients v_i^* . Furthermore, we define the \mathcal{T}^* -piecewise constant interpolation operator

$$\mathcal{I}_h^* : \mathcal{C}(\overline{\Omega}) \rightarrow \mathcal{P}^0(\mathcal{T}^*), \quad \mathcal{I}_h^* v := \sum_{a_i \in \mathcal{N}} v(a_i) \chi_i^*(x). \quad (7)$$

3.2. The discrete system. With these preparations made we can introduce the non-symmetric FVM-BEM coupling method, which reads: find $u_h \in \mathcal{S}^1(\mathcal{T})$ and $\phi_h \in \mathcal{P}^0(\mathcal{E}_\Gamma)$ such that

$$\mathcal{A}_V(u_h, v_h) - \langle \phi_h, \mathcal{I}_h^* v_h \rangle_\Gamma = (f, \mathcal{I}_h^* v_h)_\Omega + \langle t_0, \mathcal{I}_h^* v_h \rangle_\Gamma, \quad (8a)$$

$$\langle \psi_h, (1/2 - \mathcal{K})u_h \rangle_\Gamma + \langle \psi_h, \mathcal{V}\phi_h \rangle_\Gamma = \langle \psi_h, (1/2 - \mathcal{K})u_0 \rangle_\Gamma \quad (8b)$$

for all $v_h \in \mathcal{S}^1(\mathcal{T})$, $\psi_h \in \mathcal{P}^0(\mathcal{E}_\Gamma)$ with the finite volume bilinear form $\mathcal{A}_V : \mathcal{S}^1(\mathcal{T}) \times \mathcal{S}^1(\mathcal{T}) \rightarrow \mathbb{R}$ given by

$$\begin{aligned} \mathcal{A}_V(u_h, v_h) := \sum_{a_i \in \mathcal{N}} v_h(a_i) & \left(\int_{\partial V_i \setminus \Gamma} (-\mathbf{A} \nabla u_h + \mathbf{b} u_h) \cdot \mathbf{n} \, ds \right. \\ & \left. + \int_{V_i} c u_h \, dx + \int_{\partial V_i \cap \Gamma^{out}} \mathbf{b} \cdot \mathbf{n} u_h \, ds \right). \end{aligned} \quad (9)$$

A more detailed derivation can be found in [EOS15].

Remark 1. *Note that the trial and test spaces are in fact different.*

It is well known that the FVM with the central approximation of the convection term leads to strong instabilities for convection dominated problems. Finite volume schemes, however, allow an easy upwind stabilization; see [RST96]. Although there exist several upwinding possibilities, we focus on the classical full upwinding in this work.

If we want to apply an upwind scheme for the finite volume scheme, we replace $\mathbf{b} u_h$ on the interior dual edges/faces $V_i \setminus \Gamma$ in \mathcal{A}_V (9) by an upwind approximation. Given $V_i \in \mathcal{T}^*$, we consider the intersections with the neighboring boxes $\tau_{ij} = V_i \cap V_j \neq \emptyset$ for $V_j \in \mathcal{T}^*$. Note that in two dimensions τ_{ij} is the union of two straight segments or (when the associated vertices $a_i, a_j \in \mathcal{N}$ lie on Γ) a single segment; see Figure 1(b). In three dimensions τ_{ij} consists of one or two polygonal surfaces. We then compute the average

$$\beta_{ij} := \frac{1}{|\tau_{ij}|} \int_{\tau_{ij}} \mathbf{b} \cdot \mathbf{n}_i \, ds,$$

where \mathbf{n}_i points outwards with respect to V_i . Then, the upwind value $u_{h,ij}$ defined by the classical (full) upwind scheme is

$$u_{h,ij} := \begin{cases} u_h(a_j) & \text{for } \beta_{ij} < 0, \\ u_h(a_i) & \text{for } \beta_{ij} \geq 0. \end{cases} \quad (10)$$

The analysis in this work also holds for a weighted upwinding strategy which is used to reduce the excessive numerical diffusion; see [RST96, EOS15].

Whenever we apply an upwind scheme for the convection part, we replace the finite volume bilinear form \mathcal{A}_V in (8a) by

$$\begin{aligned} \mathcal{A}_V^{up}(u_h, v_h) := \sum_{a_i \in \mathcal{N}} v_h(a_i) & \left(\int_{\partial V_i \setminus \Gamma} -\mathbf{A} \nabla u_h \cdot \mathbf{n} \, ds + \int_{V_i} c u_h \, dx \right. \\ & \left. + \sum_{j \in \mathcal{N}_i} \int_{\tau_{ij}} \mathbf{b} \cdot \mathbf{n} u_{h,ij} \, ds + \int_{\partial V_i \cap \Gamma^{out}} \mathbf{b} \cdot \mathbf{n} u_h \, ds \right). \end{aligned} \quad (11)$$

where \mathcal{N}_i denotes the index set of nodes in \mathcal{T} of all neighbors of $a_i \in \mathcal{N}$.

4. RESIDUAL BASED A POSTERIORI ERROR ESTIMATOR

In this section we will introduce an elementwise refinement indicator on which our a posteriori error estimator is based. In order to do that we define the residual

$$R := R(u_h) = f - \operatorname{div}(-\mathbf{A} \nabla u_h + \mathbf{b} u_h) - c u_h \quad \text{on } T \in \mathcal{T} \quad (12)$$

and an edge/face-residual or jump $J : L^2(\mathcal{E}) \rightarrow \mathbb{R}$ by

$$J|_E := J(u_h)|_E = \begin{cases} [(-\mathbf{A}\nabla u_h)|_{E,T} - (-\mathbf{A}\nabla u_h)|_{E,T'}] \cdot \mathbf{n} & \text{for all } E \in \mathcal{E}_I \text{ with} \\ & E = T \cap T', T, T' \in \mathcal{T} \\ (-\mathbf{A}\nabla u_h + \mathbf{b}u_h) \cdot \mathbf{n} + \phi_h + t_0 & \text{for all } E \in \mathcal{E}_\Gamma^{in}, \\ -\mathbf{A}\nabla u_h \cdot \mathbf{n} + \phi_h + t_0 & \text{for all } E \in \mathcal{E}_\Gamma^{out}. \end{cases} \quad (13)$$

Note that $\varphi_{E,T}$ denotes the trace of $\varphi \in H^1(T)$ on E and the normal vector \mathbf{n} points from T to T' .

4.1. Robust a posteriori estimation. For analytical investigations we define the energy (semi)norm

$$\|v\|_\Omega^2 := \|\mathbf{A}^{1/2}\nabla v\|_{L^2(\Omega)}^2 + \left\| \left(\frac{1}{2} \operatorname{div} \mathbf{b} + c \right)^{1/2} v \right\|_{L^2(\Omega)}^2 \quad \text{for all } v \in H^1(\Omega). \quad (14)$$

We stress that there holds with (2) and $\mathbf{b} \cdot \mathbf{n} \leq 0$ on Γ^{in}

$$\|v\|_\Omega^2 \leq \mathcal{A}(v, v). \quad (15)$$

The following lemma is the key observation for showing a robust upper estimate.

Lemma 2. *Let us assume $0 < \varepsilon < 1$ and $(1 - \varepsilon)\lambda_{\min}(\mathbf{A}) - \frac{1}{4}C_K > 0$. For all $\mathbf{v} = (v, \psi) \in \mathcal{H}$ there holds*

$$\mathcal{B}(\mathbf{v}; \mathbf{v}) \geq \min\{\varepsilon, C_{\text{harm}}\} \left(\|v\|_\Omega^2 + \|\psi\|_{\mathcal{V}}^2 \right) \quad (16)$$

with the constant

$$C_{\text{harm}} = \frac{1}{2} \left[(1 - \varepsilon)\lambda_{\min}(\mathbf{A}) + 1 - \sqrt{((1 - \varepsilon)\lambda_{\min}(\mathbf{A}) - 1)^2 + C_K} \right]$$

and the contraction constant $C_K \in [1/2, 1)$.

Proof. The proof is similar to the proof in [EOS15, Theorem 4]. Thus we only sketch the steps that differ. In the following we denote by $S^{\text{int}} := \mathcal{V}^{-1}(1/2 + \mathcal{K})$ the Steklov–Poincaré operator, i.e., the Dirichlet to Neumann map of the interior Laplace problem. Let $\mathbf{v} = (v, \psi) \in \mathcal{H}$ be arbitrary. Thus, (4), the contractivity property $\langle \psi, (1/2 + \mathcal{K})v \rangle_\Gamma \leq C_K^{1/2} \langle S^{\text{int}}v, v \rangle_\Gamma^{1/2} \|\psi\|_{\mathcal{V}}$, the ellipticity (15) of $\mathcal{A}(v, v)$ in the (semi)energy norm (14), and the ellipticity of \mathcal{V} lead to

$$\begin{aligned} \mathcal{B}(\mathbf{v}; \mathbf{v}) &= \mathcal{A}(v, v) + \langle \psi, \mathcal{V}\psi \rangle_\Gamma - \langle \psi, (1/2 + \mathcal{K})v \rangle_\Gamma \\ &\geq \|\mathbf{A}^{1/2}\nabla v\|_{L^2(\Omega)}^2 + \|((\operatorname{div} \mathbf{b})/2 + c)^{1/2}v\|_{L^2(\Omega)}^2 + \|\psi\|_{\mathcal{V}}^2 - C_K^{1/2} \langle S^{\text{int}}v, v \rangle_\Gamma^{1/2} \|\psi\|_{\mathcal{V}} \end{aligned}$$

Next, for $0 < \varepsilon < 1$ we split $\|\mathbf{A}^{1/2}\nabla v\|_{L^2(\Omega)}^2 = \varepsilon\|\mathbf{A}^{1/2}\nabla v\|_{L^2(\Omega)}^2 + (1 - \varepsilon)\|\mathbf{A}^{1/2}\nabla v\|_{L^2(\Omega)}^2$. With harmonic splitting we build a quadratic form as in [EOS15, Theorem 4]. Thus, under the assumption that $(1 - \varepsilon)\lambda_{\min}(\mathbf{A}) - \frac{1}{4}C_K > 0$, $\langle S^{\text{int}}v, v \rangle_\Gamma \geq 0$, and with the constant C_{harm} we estimate

$$\mathcal{B}(\mathbf{v}; \mathbf{v}) \geq \varepsilon\|\mathbf{A}^{1/2}\nabla v\|_{L^2(\Omega)}^2 + \|((\operatorname{div} \mathbf{b})/2 + c)^{1/2}v\|_{L^2(\Omega)}^2 + C_{\text{harm}}\|\psi\|_{\mathcal{V}}^2,$$

which proves the assertion. \square

Note that (16) allows us to prove a robust upper bound. However, the diffusion distribution in Ω has to be quasi-monotone to apply a robust interpolant; see also [Pet02] in the context of an FEM estimator and [Era13b] for an FVM-BEM estimator. To simplify notation, we restrict ourself to a piecewise constant diffusion coefficient $\alpha \in \mathcal{P}^0(\mathcal{T})$ with $\mathbf{A} = \alpha \mathbf{I}$. Let us suppose that Ω can be partitioned into a finite number L of open disjoint subdomains Ω_ℓ , $1 \leq \ell \leq L$ such that the function α is equal to a constant $\alpha_\ell \in \mathbb{R}$ on each Ω_ℓ and the triangulation \mathcal{T} of Ω fits to Ω_ℓ ; i.e., $\partial\Omega_\ell$ consists of edges of the underlying triangulation. Thus, for two subdomains Ω_k, Ω_ℓ with $\partial\Omega_k \cap \partial\Omega_\ell \neq \emptyset$ we may assume $\alpha_k \neq \alpha_\ell$. Otherwise, one can merge Ω_k and Ω_ℓ with $\alpha_k = \alpha_\ell$ to a new subdomain. For the \mathcal{T} -piecewise constant function $\alpha \in \mathcal{P}^0(\mathcal{T})$ we write

$$\alpha_T := \alpha|_T \quad \text{for all } T \in \mathcal{T},$$

which obviously gives $\alpha_T = \alpha_\ell$ in Ω_ℓ .

With the definition of the patch of a node $a \in \mathcal{N}$ via

$$\omega_a := \bigcup_{T \in \tilde{\omega}_a} T \quad \text{with } \tilde{\omega}_a := \{T \in \mathcal{T} \mid a \in \partial T\},$$

we can define the set

$$Q_a := \bigcup_{T \in \tilde{Q}_a} T, \quad \text{where } \tilde{Q}_a := \{T \in \tilde{\omega}_a \mid \alpha_T \geq \alpha_{T'}, \text{ for all } T' \in \tilde{\omega}_a\}.$$

Note that Q_a denotes the union of all simplexes $T \in \tilde{\omega}_a$ for $a \in \mathcal{N}$, where α_T achieves a maximum.

Definition 3 (Quasi-monotonicity [Pet02, Era13b]). *Let $a \in \mathcal{N}$. We say α is quasi-monotone in ω_a with respect to a , if for all elements $T \in \tilde{\omega}_a$ there exists a simply connected set $Q_{a,T}$ with $T \cup Q_a \subset Q_{a,T} \subset \omega_a$ such that $\alpha_T \leq \alpha_{T'}$ for all $T' \subset Q_{a,T}$, $T' \in \tilde{\omega}_a$. We call α quasi-monotone, if α is quasi-monotone for all $a \in \mathcal{N}$.*

The definitions of [Pet02] and [Era13b] slightly differ, since the coupling does not have a Dirichlet boundary. This allows us to define a robust nodal interpolant in the sense of [Pet02];

$$\mathcal{I}_h : H^1(\Omega) \rightarrow \mathcal{S}^1(\mathcal{T}), \quad \mathcal{I}_h v := \sum_{a \in \mathcal{N}} \Pi_a v \eta_a, \quad (17)$$

well known in the context of the finite element method. Here η_a is the standard nodal linear basis function associated with the node a . The linear and continuous operator $\Pi_a : H^1(\omega) \rightarrow \mathbb{R}$ on a domain $\omega \subset \Omega$ for a diffusion coefficient with a quasi-monotone distribution reads

$$\Pi_a v := \frac{1}{|Q_a|} \int_{Q_a} v \, dx.$$

Before we can introduce a robust refinement indicator, we need some more notation: First, we define

$$\begin{aligned} \alpha_E &:= \max \{ \alpha_{T_1}, \alpha_{T_2} \} & \text{for } E \in \mathcal{E}_I \text{ with } E \subset T_1 \cap T_2, \\ \alpha_E &:= \alpha_T & \text{for } E \in \mathcal{E}_\Gamma \text{ with } E \subset \partial T. \end{aligned}$$

Besides α_E we define additional quantities; i.e.,

$$\begin{aligned}\beta_T &:= \min_{x \in T} \left\{ \frac{1}{2} \operatorname{div} \mathbf{b}(x) + c(x) \right\} & \text{for all } T \in \mathcal{T}, \\ \beta_E &:= \min \{ \beta_{T_1}, \beta_{T_2} \} & \text{for } E \in \mathcal{E}_I \text{ with } E \subset T_1 \cap T_2, \\ \beta_E &:= \beta_T & \text{for } E \in \mathcal{E}_\Gamma \text{ with } E \subset \partial T.\end{aligned}$$

Next, we define $\mu_T := \min \{ \beta_T^{-1/2}, h_T \alpha_T^{-1/2} \}$ for all $T \in \mathcal{T}$ and $\mu_E := \min \{ \beta_E^{-1/2}, h_E \alpha_E^{-1/2} \}$ for all $E \in \mathcal{E}$. As a notational convention, we take the second argument if $\beta_T = 0$ or $\beta_E = 0$. Then, the robust refinement indicator reads for all $T \in \mathcal{T}$

$$\begin{aligned}\eta_T^2 &:= \mu_T^2 \|R\|_{L^2(T)}^2 + \frac{1}{2} \sum_{E \in \mathcal{E}_I \cap \mathcal{E}_T} \alpha_E^{-1/2} \mu_E \|J\|_{L^2(E)}^2 + \sum_{E \in \mathcal{E}_\Gamma \cap \mathcal{E}_T} \alpha_E^{-1/2} \mu_E \|J\|_{L^2(E)}^2 \\ &+ \sum_{E \in \mathcal{E}_\Gamma \cap \mathcal{E}_T} h_E \|\nabla_\Gamma((1/2 - \mathcal{K})(u_0 - u_h) - \mathcal{V}\phi_h)\|_{L^2(E)}^2\end{aligned}\tag{18}$$

with R and J from (12) and (13), respectively. If we apply the upwind discretization (11) we additionally need for all $T \in \mathcal{T}$

$$\eta_{T,up}^2 := \alpha_T^{-1/2} \mu_T \sum_{\tau_{ij}^T \in \mathcal{D}^T} \|\mathbf{b} \cdot \mathbf{n}_i(u_h - u_{h,ij})\|_{L^2(\tau_{ij}^T)}^2\tag{19}$$

with $\mathcal{D}^T := \{ \tau_{ij}^T \mid \tau_{ij}^T = V_i \cap V_j \cap T \text{ for } V_i, V_j \in \mathcal{T}^* \text{ with } V_i \neq V_j, V_i \cap T \neq \emptyset, V_j \cap T \neq \emptyset \}$ and $u_{h,ij}$ from (10). To prove robustness of our a posteriori estimator we use the following L^2 -orthogonality property, which will help us to overcome the lack of Galerkin orthogonality of the FVM part, and some robust estimates of the residual and jump terms from [Era13b];

Lemma 4 ([Era13b]). *Let \mathcal{I}_h be the robust nodal interpolant (17) for quasi-monotone diffusion distribution in the sense of [Pet02] and \mathcal{I}_h^* the \mathcal{T}^* -piecewise constant interpolation operator (7). With the notation above there holds*

- for all $v^* \in \mathcal{P}^0(\mathcal{T}^*)$

$$\sum_{T \in \mathcal{T}} \int_T R v^* dx + \sum_{E \in \mathcal{E}} \int_E J v^* ds = 0.\tag{20}$$

- for all $v \in H^1(\Omega)$, and $v_h = \mathcal{I}_h v \in \mathcal{S}^1(\mathcal{T})$

$$\sum_{T \in \mathcal{T}} \int_T R(v - v_h) dx \lesssim \left(\sum_{T \in \mathcal{T}} \min \{ \beta_T^{-1}, h_T^2 \alpha_T^{-1} \} \|R\|_{L^2(T)}^2 \right)^{1/2} \|v\|_\Omega,\tag{21}$$

$$\sum_{E \in \mathcal{E}} \int_E J(v - v_h) ds \lesssim \left(\sum_{E \in \mathcal{E}} \alpha_E^{-1/2} \min \{ \beta_E^{-1/2}, h_E \alpha_E^{-1/2} \} \|J\|_{L^2(E)}^2 \right)^{1/2} \|v\|_\Omega.\tag{22}$$

- for all $v \in H^1(\Omega)$, $v_h = \mathcal{I}_h v \in \mathcal{S}^1(\mathcal{T})$, and $v_h^* = \mathcal{I}_h^* v_h \in \mathcal{P}^0(\mathcal{T}^*)$

$$\sum_{T \in \mathcal{T}} \int_T R(v_h - v_h^*) dx \lesssim \left(\sum_{T \in \mathcal{T}} \min \{ \beta_T^{-1}, h_T^2 \alpha_T^{-1} \} \|R\|_{L^2(T)}^2 \right)^{1/2} \|v\|_\Omega, \quad (23)$$

$$\sum_{E \in \mathcal{E}} \int_E J(v_h - v_h^*) ds \lesssim \left(\sum_{E \in \mathcal{E}} \alpha_E^{-1/2} \min \{ \beta_E^{-1/2}, h_E \alpha_E^{-1/2} \} \|J\|_{L^2(E)}^2 \right)^{1/2} \|v\|_\Omega. \quad (24)$$

The next lemma describes the localization of the Sobolev norm on the boundary. It is well-known in the context of a posteriori estimates for boundary element methods; e.g., [Car97, Theorem 1] for the two dimensional case and [CMS01, Theorem 3.2 and Corollary 4.2] for the three dimensional case. In the following, ∇_Γ denotes the arc length derivative in the 2-D case or the gradient over the surface in the 3-D case.

Lemma 5. *Assume $v \in H^1(\Gamma)$ is $L^2(\Gamma)$ -orthogonal to $\mathcal{P}^0(\mathcal{E}_\Gamma)$. Then, there holds*

$$\|v\|_{H^{1/2}(\Gamma)} \leq C(\mathcal{E}_\Gamma) \left(\sum_{E \in \mathcal{E}_\Gamma} h_E \|\nabla_\Gamma v\|_{L^2(E)}^2 \right)^{1/2}. \quad (25)$$

Remark 6. The constant $C(\mathcal{E}_\Gamma)$ depends on the (boundary-) mesh \mathcal{E}_Γ , but we can ensure its boundedness by shape regularity of \mathcal{T} in two dimensions and by only using newest vertex bisection refinement in the 3-D case. We refer to [CMS01] for a detailed discussion about the dependency.

Standard techniques for residual-based error estimates together with Lemmas 2, 4 and 5 allow us to show:

Theorem 7 (Robust reliability). *Let us assume $0 < \varepsilon < 1$ and $(1 - \varepsilon)\alpha_{\min} - \frac{1}{4}C_\mathcal{K} > 0$, where $\alpha_{\min} = \min_{T \in \mathcal{T}} \alpha_T$. Then, there is a constant $C_{\text{rel}} > 0$ which depends only on the shape of the elements in \mathcal{T} but not on the size, the number of elements nor the variation of the model data such that*

$$\|u - u_h\|_\Omega + \|\phi - \phi_h\|_\mathcal{V} \leq C_{\text{rel}} \frac{1}{\min \{ \varepsilon, C_{\text{harm}} \}} \left(\sum_{T \in \mathcal{T}} \eta_T^2 \right)^{1/2} \quad (26)$$

with

$$C_{\text{harm}} = \frac{1}{2} \left[(1 - \varepsilon)\alpha_{\min} + 1 - \sqrt{((1 - \varepsilon)\alpha_{\min} - 1)^2 + C_\mathcal{K}} \right]$$

If we replace \mathcal{A}_V by \mathcal{A}_V^{up} (11) in (8) we get the robust upper bound

$$\|u - u_h\|_\Omega + \|\phi - \phi_h\|_\mathcal{V} \leq C_{\text{rel}} \frac{1}{\min \{ \varepsilon, C_{\text{harm}} \}} \left(\sum_{T \in \mathcal{T}} (\eta_T^2 + \eta_{T,up}^2) \right)^{1/2}. \quad (27)$$

Remark 8. The constant $1/\min \{ \varepsilon, C_{\text{harm}} \}$ needs some discussion. First we note that if $\alpha_{\min} > C_\mathcal{K}/(4(1 - \varepsilon))$ then $C_{\text{harm}} > 0$ and if $\alpha_{\min} \rightarrow C_\mathcal{K}/(4(1 - \varepsilon))$ then $C_{\text{harm}} \rightarrow 0$ (monotone). Thus, if we want to guarantee $1/\min \{ \varepsilon, C_{\text{harm}} \} = 1/\varepsilon$, we have the constraint

$$\alpha_{\min} > \frac{4\varepsilon(1 - \varepsilon) + C_\mathcal{K}}{4(1 - \varepsilon)^2}.$$

Note that the contraction constant $C_K \in [1/2, 1)$ depends on the shape of Ω . For example, if we set $\varepsilon = 1/10$ and pick $C_K = 1$ (worst case) Theorem 7 holds for $\alpha_{\min} > 0.4198$. Thus the reliability constant is in fact $10C_{\text{rel}}$, which is robust with respect to the jumping diffusion α , \mathbf{b} and c .

Proof. Let us write $e := u - u_h \in H^1(\Omega)$, $\delta := \phi - \phi_h \in H^{-1/2}(\Gamma)$ for the errors. Some standard transformations, (6) and integration by parts lead to

$$\begin{aligned} \mathcal{B}((e, \delta); (e, \delta)) &= (f, e)_\Omega + \langle t_0, e \rangle_\Gamma + \langle \delta, (1/2 - \mathcal{K})u_0 \rangle_\Gamma \\ &\quad - (\mathcal{A}(u_h, e) - \langle \phi_h, e \rangle_\Gamma + \langle \delta, (1/2 - \mathcal{K})u_h \rangle_\Gamma + \langle \delta, \mathcal{V}\phi_h \rangle_\Gamma) \\ &= \sum_{T \in \mathcal{T}} \int_T R e \, dx + \sum_{E \in \mathcal{E}} \int_E J e \, dx \\ &\quad + \langle \delta, (1/2 - \mathcal{K})u_0 \rangle_\Gamma - \langle \delta, (1/2 - \mathcal{K})u_h \rangle_\Gamma - \langle \delta, \mathcal{V}\phi_h \rangle_\Gamma \end{aligned}$$

For the sums with R and J we use as in [Era13b] the L^2 orthogonality (20) with $e_h^* = \mathcal{I}_h^* e_h$ where $e_h = \mathcal{I}_h e$ and add $e_h - e_h^*$. Then, Cauchy-Schwarz inequality, the use of the robust estimates (21)–(24) and the localization (25), see also (8b), lead to

$$\begin{aligned} \mathcal{B}((e, \delta); (e, \delta)) &\lesssim \left[\left(\sum_{T \in \mathcal{T}} \mu_T^2 \|R\|_{L^2(T)}^2 \right)^{1/2} + \left(\sum_{E \in \mathcal{E}} \alpha_E^{-1/2} \mu_E \|J\|_{L^2(E)}^2 \right)^{1/2} \right] \|e\|_\Omega \\ &\quad + \left(\sum_{E \in \mathcal{E}_\Gamma} h_E \|\nabla_\Gamma ((1/2 - \mathcal{K})(u_0 - u_h) - \mathcal{V}\phi_h)\|_{L^2(E)}^2 \right)^{1/2} \|\delta\|_{H^{-1/2}(\Gamma)} \end{aligned}$$

Applying the Cauchy-Schwarz inequality again and the robust estimate (16) proves the first assertion (26). To prove (27) we can use [Era13b, Lemma 5.1, Lemma 5.2] \square

4.1.1. *Non-robust reliable error estimator.* We can also give a non-robust error estimator, which can easily be defined for a diffusion matrix \mathbf{A} and is less restricting than the robust estimator.

$$\begin{aligned} \eta_T^2 &:= h_T^2 \|R\|_{L^2(T)}^2 + \frac{1}{2} \sum_{E \in \mathcal{E}_T \cap \mathcal{E}_T} h_E \|J\|_{L^2(E)}^2 + \sum_{E \in \mathcal{E}_\Gamma \cap \mathcal{E}_T} h_E \|J\|_{L^2(E)}^2 \\ &\quad + \sum_{E \in \mathcal{E}_\Gamma \cap \mathcal{E}_T} h_E \|\nabla_\Gamma ((1/2 - \mathcal{K})(u_0 - u_h) - \mathcal{V}\phi_h)\|_{L^2(E)}^2 \end{aligned} \quad (28)$$

for all $T \in \mathcal{T}$.

Theorem 9 (Reliability). *Let us assume $\lambda_{\min} - \frac{1}{4}C_K > 0$. Then, there is a constant $C_{\text{rel}} > 0$ which depends on the model data and on the shape of the elements in \mathcal{T} but not on the size or the number of elements such that*

$$\|u - u_h\|_{H^1(\Omega)} + \|\phi - \phi_h\|_{H^{-1/2}(\Gamma)} \leq C_{\text{rel}} \left(\sum_{T \in \mathcal{T}} \eta_T^2 \right)^{1/2}.$$

Proof. We will only sketch the proof as it mostly follows the lines above. A similar proof in the case of FEM-BEM coupling with $\mathbf{b} = (0, 0)^T$ and $c = 0$ can be found in [AFF⁺13]. Let us write $e := u - u_h \in H^1(\Omega)$, $\delta := \phi - \phi_h \in H^{-1/2}(\Gamma)$ for the errors. Instead of using the robust

estimate (16) we use the ellipticity of the equivalent stabilized bilinear form of [EOS15], i.e., there holds

$$\|e\|_{H^1(\Omega)} + \|\delta\|_{H^{-1/2}(\Gamma)} \lesssim \mathcal{B}((e, \delta); (e, \delta)) + \beta(\langle 1, (1/2 + \mathcal{K})e + \mathcal{V}\delta \rangle_\Gamma) = \mathcal{B}((e, \delta); (e, \delta)). \quad (29)$$

The last step follows directly from the second coupling equations (3b) and (8b). Note that the stabilization term ($\beta = 1$) is only needed if $(\operatorname{div} \mathbf{b})/2 + c = 0$ almost everywhere in Ω (otherwise $\beta = 0$). As in the proof of the robust error estimator we arrive at

$$\begin{aligned} \|e\|_{H^1(\Omega)} + \|\delta\|_{H^{-1/2}(\Gamma)} \lesssim \mathcal{B}((e, \delta); (e, \delta)) &= \sum_{T \in \mathcal{T}} \int_T Re \, dx + \sum_{E \in \mathcal{E}} \int_E Je \, dx + \langle \delta, (1/2 - \mathcal{K})u_0 \rangle_\Gamma \\ &\quad - \langle \delta, (1/2 - \mathcal{K})u_h \rangle_\Gamma - \langle \delta, \mathcal{V}\phi_h \rangle_\Gamma. \end{aligned}$$

Again, we add $e_h - e_h$ with $e_h = \mathcal{I}_h e$, where \mathcal{I}_h can be the standard Clément nodal interpolant (17) in the sense of [Clé75], and use the L^2 orthogonality (20) with $e_h^* = \mathcal{I}_h^* e_h$. The resulting terms can then be estimated by means of the Cauchy-Schwarz inequality, Clément type interpolation estimates [Clé75], and estimates of the piecewise constant nodal interpolation operator \mathcal{I}_h^* ; see [Era12, Lemma 4.1]. \square

Remark 10. The ellipticity (29) only holds for $\alpha_{\min} > C_K/4$; see Remark 8 for the robust estimate. The ellipticity constant depends on the model data and the boundary Γ and can become very small. However, this seems to be a theoretical bound; see [EOS15].

4.2. Efficiency. Following [Ver96], the analysis to prove efficiency for our residual based a posteriori error estimator needs some more regularity on the solution and the data. Thus we assume $u|_\Gamma \in H^1(\Gamma)$, $\phi \in L^2(\Gamma)$, $u_0 \in H^1(\Gamma)$ and $t_0 \in L^2(\Gamma)$. The idea is to use so called bubble functions and an edge lifting operator, which imply some inverse estimates for polynomial functions. To get a lower bound in the energy (semi)norm (14) the inverse estimates are based on bubble functions on a squeezed element; see, e.g., [Ver98, Era10]. To get a lower bound for the terms with the boundary integral operators \mathcal{V} and \mathcal{K} of (18) we require that \mathcal{T} is a quasi-uniform mesh on the boundary Γ . That means, the ratio of the longest edge in \mathcal{E}_Γ to the shortest edge in \mathcal{E}_Γ for a sequence of meshes is bounded by a constant, which does not depend on the size of the elements. Furthermore, there is only a global upper bound available. We stress that even for FEM-BEM residual estimators there is no better efficiency result available in the literature. For more details we refer to [Era10, Section 6] and [Era13b].

Lemma 11. Let $\tilde{\xi}_h \in \mathcal{S}^1(\mathcal{E}_\Gamma)$ be the nodal interpolant of $u|_\Gamma$ and $\bar{\phi} \in \mathcal{P}^0(\mathcal{E}_\Gamma)$ the \mathcal{E}_Γ -piecewise integral mean of ϕ , $h_{\Gamma, \max} := \max_{E \in \mathcal{E}_\Gamma} h_E$ and $h_{\Gamma, \min} := \min_{E \in \mathcal{E}_\Gamma} h_E$. Then, there holds the

global estimate

$$\begin{aligned}
& \sum_{E \in \mathcal{E}_\Gamma} h_E^{1/2} \|\nabla_\Gamma((1/2 - \mathcal{K})(u_0 - u_h) - \mathcal{V}\phi_h)\|_{L^2(E)} \\
& \leq \sum_{E \in \mathcal{E}_\Gamma} h_E^{1/2} \left(\|\nabla_\Gamma((1/2 + \mathcal{K})(u|_\Gamma - u_h))\|_{L^2(\Gamma)} + \|\nabla_\Gamma \mathcal{V}(\phi - \phi_h)\|_{L^2(\Gamma)} \right) \\
& \lesssim \frac{h_{\Gamma, \max}^{1/2}}{h_{\Gamma, \min}^{1/2}} \left(\|u - u_h\|_{H^1(\Omega)} + \|\phi - \phi_h\|_{H^{-1/2}(\Gamma)} \right. \\
& \quad \left. + h_{\Gamma, \max}^{1/2} (\|u|_\Gamma - \tilde{\xi}_h\|_{H^1(\Gamma)} + \|\phi - \bar{\phi}\|_{L^2(\Gamma)}) \right).
\end{aligned}$$

Proof. The first inequality uses the relation $(1/2 - \mathcal{K})u_0 = (1/2 - \mathcal{K})u|_\Gamma + \mathcal{V}\phi \in H^1(\Gamma)$ and the triangle inequality. With $\|u|_\Gamma - u_h\|_{H^{1/2}(\Gamma)} \lesssim \|u - u_h\|_{H^1(\Omega)}$ the second estimate follows directly from [Era10]. \square

Finally we are able to formulate an efficiency statement for our a posteriori error estimator, i.e., η is a lower bound of the error.

Theorem 12 (Efficiency). *If \mathcal{T} is a quasi-uniform mesh on the boundary Γ , we get an inverse inequality to the reliability Theorem 7; i.e., the a posteriori estimate is sharp up to higher order terms. The quantities generated through the interior problem approximation are even locally efficient without any restriction on the boundary mesh.*

Proof. Lower estimates for the contributions with the residual R and the jump terms J of the refinement indicator η_T in (18) can be found in [Era13b, Claim 1 – Claim 4]. For terms with the boundary integral operators \mathcal{V} and \mathcal{K} of (18) we apply Lemma 11. Then, the efficiency Theorem 12 can be shown up to higher order terms. See also Remark 13. \square

Remark 13. *For a detailed discussion of the higher order terms on the right-hand side of the lower bound we refer to [Era13b, Era10]. We note that the estimate depends on the local Péclet number, which is a typical behaviour of such problems in the energy norm; see also the discussion about robustness in [Era13b, Remark 6.1] for the three field FVM-BEM coupling. Obviously, Theorem 12 holds also for the inverse inequality of the reliability Theorem 9 with the non-robust refinement indicator (28).*

5. NUMERICAL RESULTS

To verify the analytical findings and to show the strength of an adaptive refinement strategy, we present three examples in two dimensions. The calculations were done in MATLAB using some functions from the HILBERT-package [AEF⁺13] for the matrices resulting from the integral operators \mathcal{V} and \mathcal{K} . The arc-length derivative in the error estimator is estimated by a central difference quotient, thus by

$$\nabla_\Gamma v(x) \approx \frac{v(x_2) - v(x_1)}{|x_2 - x_1|}$$

with $|x_2 - x_1| = h_E/20$ and $x = (x_2 + x_1)/2$. If there is any convection involved we will use the full upwind scheme (10) and replace the bilinear form \mathcal{A}_V in (8a) by \mathcal{A}_V^{up} defined in (11).

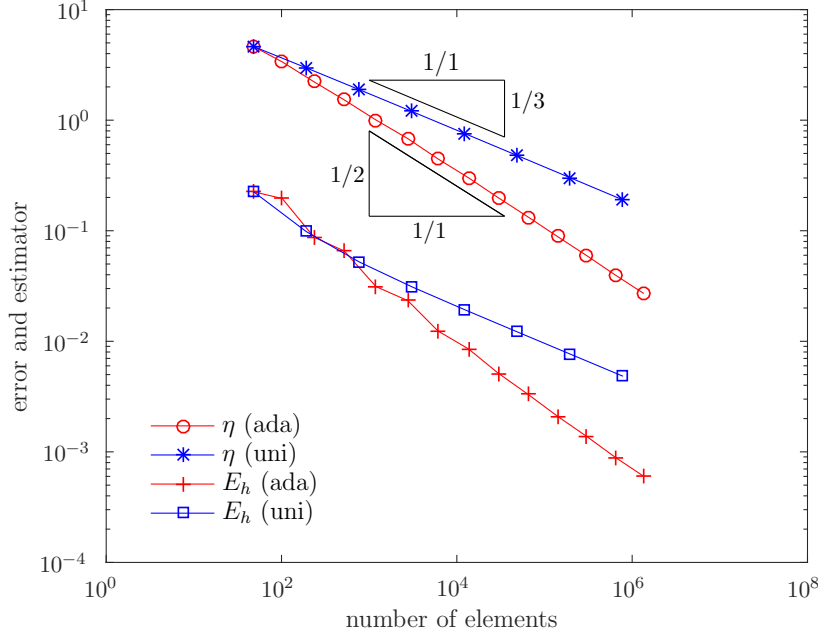


FIGURE 2. The error estimator η and the error E_h in the case of uniform (uni) and adaptive (ada) mesh refinement for the example in subsection 5.1. The recovery of the optimal convergence rate in the adaptive case can be seen.

The error will be denoted by E_h , defined as

$$E_h := \|u - u_h\|_{\Omega} + \|\phi - \phi_h\|_{\mathcal{V}}$$

(recall that $\|\cdot\|_{H^{-1/2}} \sim \|\cdot\|_{\mathcal{V}}$) and the error estimator η is given by the sum of the indicators from (18)–(19) or (28)

$$\eta := \sum_{T \in \mathcal{T}} (\eta_T^2 (+ \eta_{T,up}^2))^{1/2},$$

where the $\eta_{T,up}^2$ part is added when an upwind stabilization is used.

We will apply the refinement algorithm introduced in [Dör96] with the following marking criterion: let $\theta \in (0, 1)$, then at the refinement step k choose $\mathcal{M}^{(k)} \subset \mathcal{T}^{(k)}$ with minimal cardinality such that

$$\sum_{T \in \mathcal{M}^{(k)}} (\eta_T^2 (+ \eta_{T,up}^2)) \geq \theta \sum_{T \in \mathcal{T}^{(k)}} (\eta_T^2 (+ \eta_{T,up}^2)).$$

The elements in the subset $\mathcal{M}^{(k)}$ will then be refined by a red-green-blue refinement strategy, which leads to refined mesh $\mathcal{T}^{(k+1)}$; see also [Ver96]). Therefore, the shape regularity constant is bounded in all of our examples. We choose $\theta = 1/2$ for adaptive mesh refinement, $\theta = 1$ means uniform refinement. The regular initial triangulation $\mathcal{T}^{(0)}$ will always have triangles with approximately the same size.

5.1. Diffusion problem on an L-shaped domain. As a first test we consider a purely diffusive problem of model problem (1), i.e., without any convection or reaction, $\mathbf{b} = (0, 0)^T$

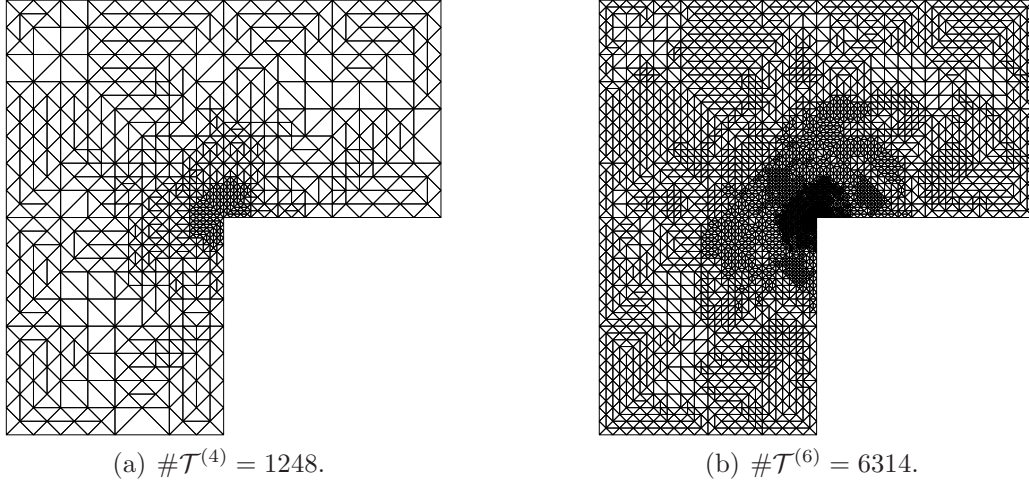


FIGURE 3. Two adaptively generated meshes $\mathcal{T}^{(4)}$ and $\mathcal{T}^{(6)}$ of the fourth and sixth refinement step of the example in subsection 5.1. The refinement mainly takes place around the singularity.

and $c = 0$, but a diffusion matrix. We want to have a specific solution to this problem. So we prescribe the coefficients and right-hand side appropriately. The domain will be L-shaped, i.e., $\Omega = (-1/4, 1/4)^2 \setminus [0, 1/4] \times [-1/4, 0]$. We prescribe a function that has a singularity in the corner $(0, 0)$ of our domain (the gradient tends to infinity at this point). The analytical solution in the interior domain Ω will then read (in polar coordinates $(x_1, x_2) = r(\cos \varphi, \sin \varphi)$ with $r \in \mathbb{R}_+$ and $\varphi \in [0, 2\pi)$)

$$u(x_1, x_2) = r^{2/3} \sin(2\varphi/3),$$

and in the exterior domain Ω_e

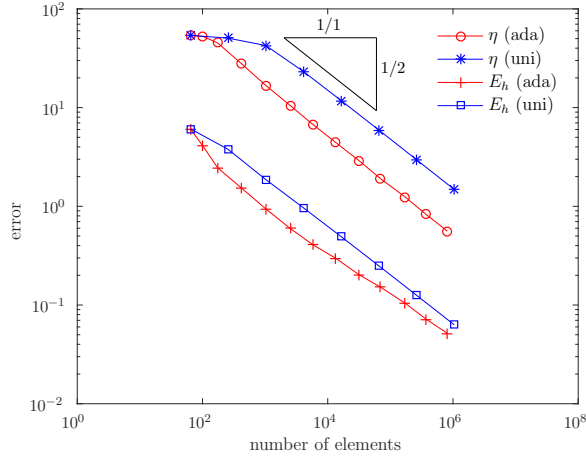
$$u_e(x_1, x_2) = \log \sqrt{(x_1 + 0.125)^2 + (x_2 - 0.125)^2}.$$

Furthermore, we will fix the diffusion matrix to

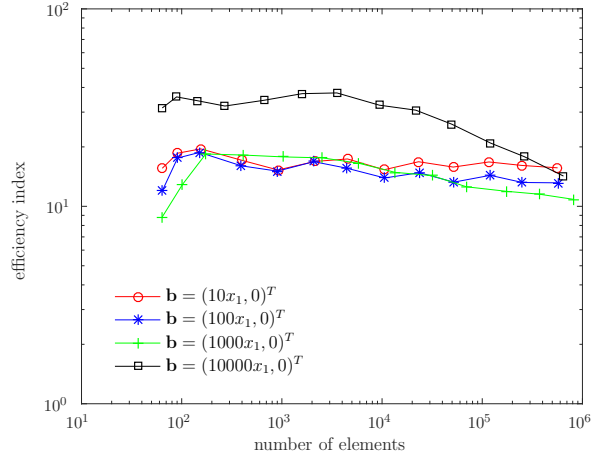
$$\mathbf{A} = \begin{pmatrix} 10 + \cos x_1 & 160 x_1 x_2 \\ 160 x_1 x_2 & 10 + \sin x_2 \end{pmatrix}.$$

We compute f and the jumps t_0 and u_0 according to the formulas.

Note that the function u is not in $H^2(\Omega)$ and thus the optimal convergence rate of $\mathcal{O}(h)$ for uniform mesh refinement [EOS15]) cannot be obtained. The notation $\mathcal{O}(h)$, where h is the minimal diameter of an element of the mesh, is a bit misleading in the adaptive case. Therefore, we consider $\mathcal{O}(N^{-p})$, where N is the number of elements and $p \in \mathbb{R}^+$, which is equivalent to $\mathcal{O}(h^p)$ for uniform mesh refinement. Figure 2 shows the error and error estimator for uniform and adaptive mesh refinement. For uniform refinement we observe the reduced convergence order $\mathcal{O}(N^{-1/3})$, whereas with our adaptive strategy we can recover the optimal rate $\mathcal{O}(N^{-1/2})$. This classical benchmark result matches observations from the literature. Note that in both cases the estimator is reliable and efficient. Figure 3 shows two adaptively generated meshes, $\mathcal{T}^{(4)}$ and $\mathcal{T}^{(6)}$, generated from a start mesh $\mathcal{T}^{(0)}$ with 48 elements. The refinement mainly takes place around the singularity.

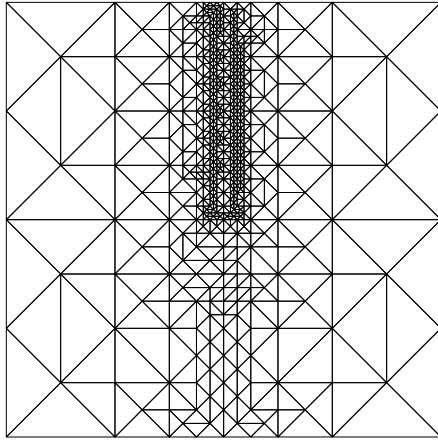


(a) Error estimator η and energy error E_h .

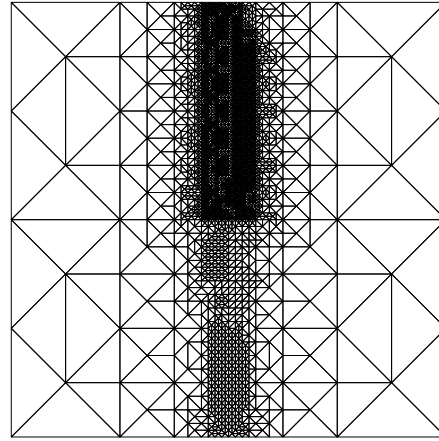


(b) Efficiency index η/E_h .

FIGURE 4. In the left figure the error estimator η and the error for the example in subsection 5.2 are shown in the case of uniform (uni) and adaptive (ada) mesh refinement. Because of the smoothness of the solution, the convergence rate is optimal also with uniform refinement. In the right figure, the efficiency index for different values for \mathbf{b} is shown.



(a) $\#\mathcal{T}^{(4)} = 1034$.



(b) $\#\mathcal{T}^{(6)} = 5846$.

FIGURE 5. Two adaptively generated meshes $\mathcal{T}^{(4)}$ and $\mathcal{T}^{(6)}$ of the fourth and sixth refinement step of the example in subsection 5.2. The refinement is mainly at the artificial shock of the analytical solution.

5.2. Diffusion-convection problem. For the next example we prescribe again a solution with known analytical properties for the model problem (1). Now we choose $\Omega = (0, 1/2) \times (0, 1/2)$. The solution in the interior domain Ω will be chosen to be

$$u(x_1, x_2) = 0.5 \left(1 - \tanh \left(\frac{0.25 - x_1}{0.02} \right) \right),$$

and the solution in the exterior domain Ω_e is similar as before, i.e.,

$$u_e(x_1, x_2) = \log \sqrt{(x_1 - 0.25)^2 + (x_2 - 0.25)^2}.$$

Thus, the interior solution has a simulated shock in the middle of the domain. We choose the jumping diffusion coefficient as

$$\alpha = \begin{cases} 0.42 & \text{for } x_2 < 0.25, \\ 10 & \text{for } x_2 \geq 0.25, \end{cases}$$

the convection field $\mathbf{b} = (1000x_1, 0)^T$ and the reaction coefficient $c = 0$. So we have a convection dominated problem which will not yield a stable solution if we are not using any upwind stabilization (10). Because of that we will always use the full upwind scheme for this problem. The right-hand side f and the jumps are calculated by means of the analytical solution. Because of the smoothness of the interior and exterior solution we would expect an (optimal) convergence rate of $\mathcal{O}(N^{-1/2})$ also for uniform mesh refinement. This can be seen in Figure 4(a). For adaptive refinement we get $\mathcal{O}(N^{-1/2})$ as well but the absolute value of the error is actual smaller. Note that in both cases, uniform and adaptive mesh refinement, the estimator is reliable and efficient. The refinement (mainly) occurs where the function has its steepest gradient and is different for the two values of the diffusion coefficient, see Figure 5 for the two meshes $\mathcal{T}^{(4)}$ and $\mathcal{T}^{(6)}$ generated from a start mesh with 64 elements. In Figure 4(b) the efficiency index η/E_h , which measures how many times we have overestimated the actual error, is plotted for adaptive mesh refinement. We see indeed the robustness of our error estimator for $\mathbf{b} = \{(10x_1, 0)^T; (100x_1, 0)^T; (1000x_1, 0)^T\}$. For $\mathbf{b} = (10000x_1, 0)^T$, which is a very high convection dominated problem, we observe the dependency of the local Péclet number, i.e., once we have resolved the shock region, the efficiency constant convergences as well.

5.3. A more practical problem. For the third example we do not know an analytical solution of (1). Additionally, we replace the radiation condition (1c) by $u_e(x) = a_\infty + \mathcal{O}(1/|x|)$ for $|x| \rightarrow \infty$. Thus we have to assume the scaling condition (in two dimensions)

$$\langle \partial u_e / \partial \mathbf{n}, 1 \rangle_\Gamma = 0,$$

see [Era13b]. The constant a_∞ has to be added to the representation formula. So we have the additional term $\langle \psi_h, a_\infty \rangle_\Gamma$ on the left-hand side of (8b) and we add an equation that ensures $\langle 1, \phi_h \rangle_\Gamma = 0$. The domain will be the classical L-shaped domain as in the example in subsection 5.1. We fix the piecewise constant diffusion coefficients to

$$\alpha = \begin{cases} 0.5 & \text{for } x_1 > 0, \\ 10 & \text{for } x_2 \leq 0, \\ 50 & \text{else,} \end{cases}$$

$\mathbf{b} = (15000, 10000)^T$, and $c = 0.01$. The right-hand side will be

$$f(x_1, x_2) = \begin{cases} 50 & \text{for } -0.2 \leq x_1 \leq -0.1, \quad -0.2 \leq x_2 \leq -0.05, \\ 0 & \text{else,} \end{cases}$$

and the jumps t_0 and u_0 are set to zero. This problem is again convection dominated. Therefore, we use the full upwind stabilization (10). The convergence rate of the error

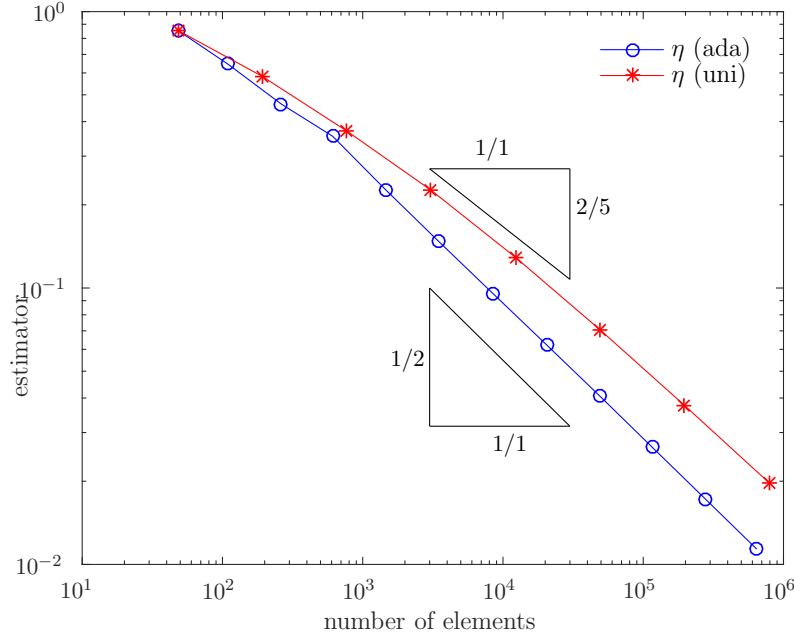


FIGURE 6. The error estimators η for the example in subsection 5.3 in the case of uniform (uni) and adaptive (ada) mesh refinement. Again we do not have the optimal convergence rate in the uniform case.

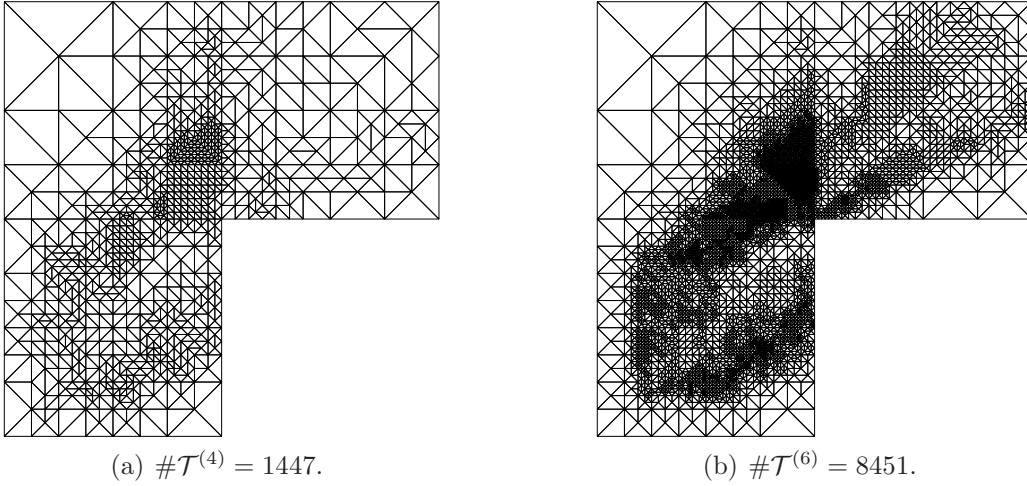


FIGURE 7. Two adaptively refined meshes $\mathcal{T}^{(4)}$ and $\mathcal{T}^{(6)}$ of the fifth and seventh step of the example in subsection 5.3. The refinement mainly takes place along the convection direction.

estimator is plotted in Figure 6. We observe a suboptimal convergence order $\mathcal{O}(N^{-2/5})$ in the uniform case. However, we can again recover the order $\mathcal{O}(N^{-1/2})$ with our adaptive strategy. Note that since we have proven the reliability and the efficiency of our error estimator, these rates depict the convergence behaviour of the error. Adaptively generated meshes $\mathcal{T}^{(4)}$ and

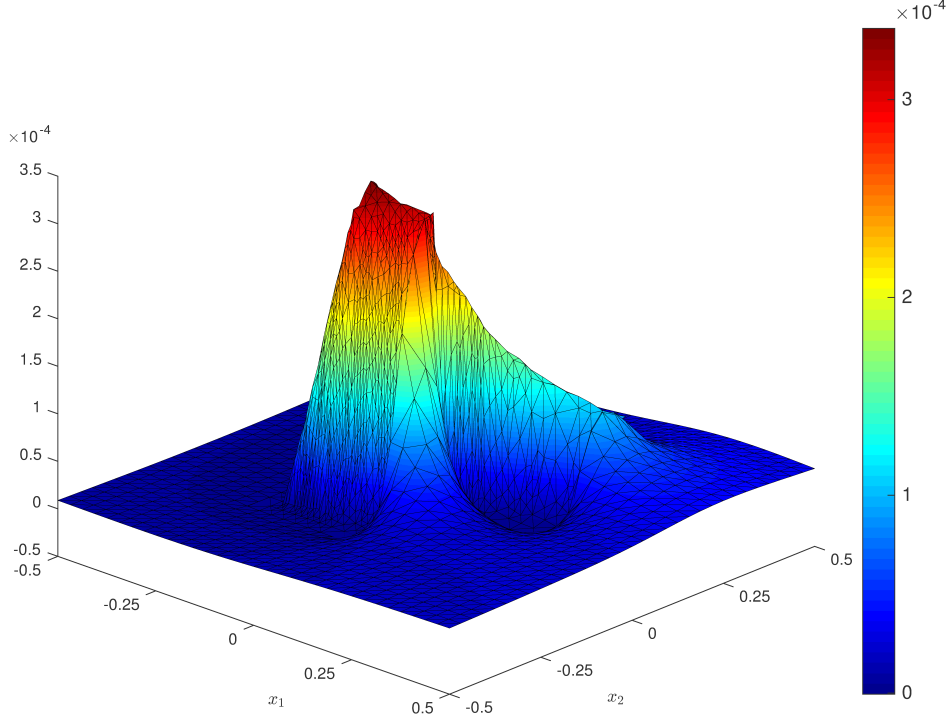


FIGURE 8. The computed solution for the example in subsection 5.3 on an adaptively generated mesh $\mathcal{T}^{(4)}$ with 3471 elements.

$\mathcal{T}^{(6)}$ from a start mesh with 48 elements are shown in Figure 7. The plots show that the mesh is the finest along the direction of the convection. Finally, in Figure 8 we see the interior and parts of the exterior discrete solution. The interior transport problem influences the exterior part, which describes a diffusion process, and the solution is continuous over the coupling boundary Γ .

6. CONCLUSIONS

This work provides an a posteriori error estimator for the non-symmetric FVM-BEM coupling discretization of [EOS15]. The error estimator bounds the error from above and, under some restrictions on the mesh, also from below. Additional assumptions even allow the construction of a robust error estimator, where the upper bound is fully robust against variation of the model data. Note that the upper estimate only holds if the diffusion is above a certain (theoretical) bound. The lower bound, however, additionally depends on the Péclet number. The analysis relies on an ellipticity estimate in the energy (semi)norm and therefore differs from the a posteriori analysis of the three field FVM-BEM coupling in [Era13b]. We think that this work and [Era13b] complete the residual based a posteriori error estimation theory for vertex-centered FVM-BEM couplings. Hence, it should be possible to transfer the results directly to Bielak-MacCamy or the symmetric coupling approaches.

ACKNOWLEDGEMENTS

The authors gratefully acknowledge Günther Of (TU Graz, Austria) for his valuable hints to show Lemma 2. The work of the second author is supported by the 'Excellence Initiative'

of the German Federal and State Governments and the Graduate School of Computational Engineering at Technische Universität Darmstadt.

REFERENCES

- [AEF⁺13] M. Aurada, M. Ebner, M. Feischl, S. Ferraz-Leite, T. Führer, P. Goldenits, M. Karkulik, M. Mayr, and D. Praetorius. HILBERT — a MATLAB implementation of adaptive 2D-BEM. *Numerical Algorithms*, 67(1):1–32, 2013.
- [AFF⁺13] M. Aurada, M. Feischl, T. Führer, M. Karkulik, J. M. Melenk, and D. Praetorius. Classical FEM-BEM coupling methods: nonlinearities, well-posedness, and adaptivity. *Computational Mechanics*, 51(4):399–419, 2013.
- [Car97] C. Carstensen. An a posteriori error estimate for a first-kind integral equation. *Math. Comp.*, 66(217):139–155, 1997.
- [Cia78] P. G. Ciarlet. *The finite element method for elliptic problems*. North-Holland Publishing Co., Amsterdam-New York-Oxford, 1978.
- [Clé75] P. Clément. Approximation by finite element functions using local regularization. *Rev. Fran caise Automat. Informat. Recherche Opérationnelle Sér. RAIRO Analyse Numérique*, 9(R-2):77–84, 1975.
- [CMS01] C. Carstensen, M. Maischak, and E. P. Stephan. A posteriori error estimate and h-adaptive algorithm on surfaces for Symm’s integral equation. *Numer. Math.*, 90(2):197–213, 2001.
- [Cos88] M. Costabel. Boundary integral operators on Lipschitz domains: elementary results. *SIAM J. Math. Anal.*, 19(3):613–626, 1988.
- [Dör96] W. Dörfler. A convergent adaptive algorithm for Poisson’s equation. *SIAM J. Numer. Anal.*, 33(3):1106–1124, 1996.
- [EOS15] C. Erath, G. Of, and F.-J. Sayas. A non-symmetric coupling of the finite volume method and the boundary element method. *Preprint, arXiv:1509.00440*, 2015.
- [Era10] C. Erath. *Coupling of the Finite Volume Method and the Boundary Element Method - Theory, Analysis, and Numerics*. PhD thesis, University of Ulm, April 2010.
- [Era12] C. Erath. Coupling of the finite volume element method and the boundary element method: an a priori convergence result. *SIAM Journal on Numerical Analysis*, 50(2):574–594, 2012.
- [Era13a] C. Erath. A new conservative numerical scheme for flow problems on unstructured grids and unbounded domains. *Journal of Computational Physics*, 245:476–492, 2013.
- [Era13b] C. Erath. A posteriori error estimates and adaptive mesh refinement for the coupling of the finite volume method and the boundary element method. *SIAM Journal on Numerical Analysis*, 51(3):1777–1804, 2013.
- [McL00] W. McLean. *Strongly elliptic systems and boundary integral equations*. Cambridge University Press, Cambridge, 2000.
- [OS13] Günther Of and Olaf Steinbach. Is the one-equation coupling of finite and boundary element methods always stable? *Z. Angew. Math. und Mech.*, 93(6-7):476–484, 2013.
- [Pet02] M. Petzoldt. A posteriori error estimators for elliptic equations with discontinuous coefficients. *Adv. Comput. Math.*, 16:47–75, 2002.
- [RST96] H. G. Roos, M. Stynes, and L. Tobiska. *Numerical methods for singularly perturbed differential equations*, volume 24. Springer, Berlin, Berlin, Heidelberg, 1996.
- [SW01] O. Steinbach and W. L. Wendland. On C. Neumann’s method for second-order elliptic systems in domains with non-smooth boundaries. *J. Math. Anal. Appl.*, 262(2):733–748, 2001.
- [Ver96] R. Verfürth. *A Review of A Posteriori Error Estimation and Adaptive Mesh-Refinement Techniques*. Wiley-Teubner, Stuttgart, 1996.
- [Ver98] R. Verfürth. A posteriori error estimators for convection-diffusion equations. *Numer. Math.*, 80(4):641–663, 1998.

TU DARMSTADT, DEPARTMENT OF MATHEMATICS, DOLIVOSTRASSE 15, 64293 DARMSTADT, GERMANY
E-mail address: `erath@mathematik.tu-darmstadt.de`

TU DARMSTADT, GRADUATE SCHOOL OF COMPUTATIONAL ENGINEERING, DOLIVOSTRASSE 15, 64293
DARMSTADT, GERMANY
E-mail address: `schorr@gsc.tu-darmstadt.de`